1. Introduction

Nitrogen oxides (NO$_x$), originated from mobile and stationary sources, are regarded as the major causes leading to global warming, ozone layer depletion, photochemical smog, acid rain and fine particles, thereby influencing the life and health of plants and animals (Lian et al., 2022). With the growing desire for good air quality, the emission reduction of NO$_x$ have been concerned many countries and areas. Chinese government issues the standard (GB 13223-2011) to limit NO$_x$ emission concentration below 100 mg/m^3 for the new coal-fired power plants and below 50 mg/m^3 for the gas turbine power plants. In addition, strict emission limits for non-electric industries, such as cement, glass and ceramic, are also required. Therefore, it is urgent to address NO$_x$ emission properly. Among numerous treatment methods (H$_2$-SCR, SNCR and NH$_3$-SCR), selective catalytic reduction (NH$_3$-SCR) of NO using NH$_3$ as one of the most effective technologies to abate NO$_x$ has been universally used in exhaust aftertreatment system (Liu et al., 2021a). Though commercial V$_2$O$_5$-WO$_3$/TiO$_2$ has been widely used to eliminate NO$_x$ to date, its further utilization in industrial production was greatly obstructed by some disadvantages, such as narrow temperature widow (300–400 °C), toxicity of vanadium and easy deactivation (Hou et al., 2021). In addition, the SCR equipment is installed in the downstream of dedusting and desulfurization units, so the flue gas temperature further decreases below 300 °C. Therefore, many researchers are dedicated to investigating low-temperature and eco-friendly SCR catalysts.

Recently, Mn-based catalysts have attracted considerable interests due to their excellent catalytic performance at low-temperature, low cost, abundance in the earth and environmentally friendly character (Choi et al., 2016; Yao et al., 2019). Among them, Cr-Mn catalysts and their ramifications, such as CrMn$_{1.5}$O$_4$ (Chen et al., 2009), MnCr$_2$O$_4$ (Gao et al., 2020b), CrMn$_2$O$_4$ (Gao et al., 2019), Ce-Mn-Cr layered double oxide (Yoon et al., 2022) and Mn$_x$Co$_{1-x}$Cr$_2$O$_4$ spinel-type catalyst (Gao et al., 2020a), exhibits outstanding low-temperature activity and wide temperature window, so they have been regarded as potential candidates for V-based catalysts during NH$_3$-SCR reactions. However, some challenges still remain when Cr-Mn catalysts and their derivatives are utilized in the post-treatment system of exhaust gases. Therein, alkali metals adsorbed on surface active sites of the catalysts could bring about a dramatic decline in catalytic performance. Hence, it is desired to investigate their poisoning mechanism by alkali metals.

In the practical industrial production, NaCl and KCl (alkali metals) in the flue gas, emitted from stationary sources (coal-fired and biomass-fired power plants), are inevitably involved in NH$_3$-SCR reactions to shorten the lifetime of SCR catalysts (Jiang et al., 2020a; Jiang et al., 2020b). According to previous experimental researches, the poisoning reasons of SCR catalysts by Na and K were concluded as followed: (1) suppressing NH$_3$ adsorption/activation by interacting with active sites or competitive adsorption, (2) forming inactive NO$_x$ species and (3) blocking pore channels and decreasing specific surface area and redox capacity (Fang et al., 2019a; Li et al., 2020; Wang et al., 2017). Furthermore, the effect of Na and K on the surface properties of SCR catalysts at atomic level was revealed by theoretical calculations. It has been reported that Na and K could adsorb on CeO$_2$-WO$_3$ catalyst (110) surface and promote surface oxygen cover active W site, thereby inhibiting NH$_3$ adsorption (Peng et al., 2012a). Some researchers revealed that K not only increased the adsorption energy for NH$_3$ on Lewis acid sites and for NH$_4^+$ on Brønsted acid sites, but also inhibited the formation of chemisorbed oxygens and oxygen vacancies (Jiang et al., 2021b). The effect of K on the SCR performance of V$_2$O$_5$/TiO$_2$ was also investigated, and it was found that K atom decreased surface acidity by accelerating electrons transfer from K to O atom, and K also led wider band gap of V$_2$O$_5$/TiO$_2$ from 0.74 to 0.81 eV, thereby decreasing its reducibility (Peng et al., 2012b).

To the best of our knowledge, most of theoretical researches focus on V-based and Ce-based catalysts, but few on promising Mn-based catalysts. The poisoning effect of Na and K, the poisoning effect of single Cl anion and the synergistic effect of Na/K and Cl on SCR catalysts are hardly revealed. Furthermore, the effect of NaCl and KCl on the rate-controlling step of L-H/*E*-R mechanism reactions is unclear. In this work, promising CrMn$_{1.5}$O$_4$ catalyst

was impregnated by various NaCl or KCl contents and used for NH$_3$-SCR of NO$_x$. Then the poisoning effect of NaCl and KCl on textural properties, crystal structure, surface atomic distribution, redox ability, surface acidity and reaction mechanism of Cr-Mn catalyst was investigated by comprehensive characterizations. Moreover, DFT calculations were carried out to reveal N$_2$ formation pathways and the poisoning effect of Na, K, Cl, NaCl and KCl on surface species at atomic level. Eventually, based on reaction pathways, we further illustrated the effect of NaCl and KCl on the rate-controlling reaction steps. This study provides a comprehensive insight into alkali metal poisoning during NH$_3$-SCR reactions and a well strategy to synthesize SCR catalysts with outstanding alkali metal resistance.

2. Experimental method

2.1. Catalyst preparation

CrMn$_{1.5}$O$_4$ catalyst (denoted as b3(t)014.3(a)03.7porixmpti18(t)ays

NH$_3$/He gas flow at 50 °C for 0.5 h. Subsequently, the samples were purged by He gases for 20 min. Finally, the samples were heated up to 800 °C at the rate of 10 °C/min in He flow. H$_2$-TPR experiments were also operated on a multifunction chemisorption analyzer (TP-5080) with TCD. The samples (0.1 g) were pretreated at 300 °C for 2 h in a steam of Ar and He. Then H$_2$/(Ar and He) mixture was fed into the reactor and the temperature increased from 100 to 800 °C at the rate of 10 °C/min. O$_2$-TPD experiments were conducted with a multifunction chemisorption analyzer (TP-5080) with TCD. Firstly, the samples (0.1 g) were pretreated O$_2$/He mixture at 280 °C for 1 h, and then cooled to 100 °C. Then the catalysts were exposed to O$_2$ for 30 min and followed by He. Finally, the temperature increased to 900 °C at the rate of 10 °C/min.

In situ DRIFTS experiments were recorded on a Brucker VERTEX 70 FTIR spectrometer and an MCT detector with a resolution of 4 cm^{-1} and 64 scan numbers. The samples were pretreated in N$_2$ flow at 400 °C for 1 h before collecting background spectra. Related test conditions consisted of 100 mL/min total gas flow, 1000 ppm NH$_3$, 1000 ppm NO, 3% O$_2$ and N$_2$ balance.

2.4. DFT calculations

CASTEP package (Materials Studio 2017R2 from Accelrys) was used to operate all calculations (Lyu et al., 2020). Generalized gradient approximation (PBE) with Perdew-Burke-Ernzerhof (PBE) functional was employed to calculate the exchange-correlation potential (Liu et al., 2021c). The ultrasoft pseudopotential was used to figure out the mutual effect of the ionic core and the valence electrons. A plane-wave basis set with the spin polarization and cutoff energy of 340 eV was applied to expand the electronic wave functions. The $(2 \times 2 \times 1)$ k-points were designed for the surface Brillouin zone integration. The convergence values during the geometry optimization and energy calculations consisted of self-consistent field energy $(1 \times 10^{-5}$ Ha$)$, atomic displacement $(5 \times 10^{-3}$ Å$)$ and energy gradient $(2 \times 10^{-3}$ Ha/Å$)$.

The adsorption energy (E$_{ads}$) for gaseous molecular and oxygen vacancy formation energy (E$_{ov}$) was defined as followed:

$$E_{ads} = E_s - E_{pf} + E_{sm}$$

$$E_{ov} = -E_{ovs} + E_o - E_{pf}$$

where E$_s$, E$_{pf}$, E$_{sm}$, E$_{ovs}$ and E$_o$ were total energy of the system after adsorption, pure facet, small molecule, oxygen vacancy system and oxygen atom, respectively.

Herein, NH$_3$-SCR reaction steps involving N$_2$ and H$_2$O formation over CM catalyst were searched by the LST/QST method (Ren et al., 2021). NH$_3$-SCR reactions contained intermediates (IM) and transition states (TS). The reaction energy barrier (E$_a$) was defined as follow:

$$E_a = E_{TS} - E_{IM1}$$

$$E_{rh} = E_{IM2} - E_{IM1}$$

where E$_{IM}$ and E$_{TS}$ were the total energy of transition states and intermediates, respectively. The smaller E$_a$ was, the more likely the reaction happened. The negative E$_{rh}$ presented that this reaction was exothermic.

In the simulation, a (2×2) periodic CrMn$_{1.5}$O$_4$ (111) slab model was originated from CrMn$_{1.5}$O$_4$ conventional cell (Fig. S1a). As shown in Fig. S1b, (111) facet as common crystal facet presented threefold-coordinated Cr atom (Cr$_{3c}$), threefold-coordinated Mn atom (Mn$_{3c}$) and threefold-coordinated O atom (O$_{3c}$). The CrMn$_{1.5}$O$_4$ slab model consisted of total 10 atomic layers, corresponding to 92 atoms. The related oxygen vacancy models were obtained by deleting an oxygen connected Cr with Mn on (111) facet surface layer. During the calculation, the bottom half atoms were immobilized, while the top half atoms and small molecules were fully relaxed with the purpose of reducing the calculation time. A 18 Å vacuum slab was set to prevent the interaction between the adjacent surface (Pan et al., 2021a).

3. Results and discussion

3.1. NH$_3$-SCR activity

NO conversion of fresh, NaCl-poisoned and KCl-poisoned CM catalysts was simultaneously measured to shed light on the poisoning effect of NaCl and KCl on the catalytic activity of CM catalyst and related results were shown in Fig. 1. Note that the NO conversion of fresh CM catalyst was 100% NO conversion within 160–240 °C, and over 90% NO conversion was acquired in the range of 148–296 °C. However, NaCl and KCl addition exhibited an obvious inhibitory effect on NO conversion in the entire temperature range. Specifically, the order of activity loss was ranked by KCl$_{0.05}$-CM>NaCl$_{0.05}$-CM>KCl$_{0.01}$-CM>NaCl$_{0.01}$-CM, indicating that both NaCl and KCl seriously poisoned CM catalyst and KCl exhibited stronger toxicity than NaCl. As shown in Fig. S2. NaCl and KCl did not almost reduce N$_2$ selectivity of CM catalyst, which might be because of reduced redox reducibility inhibiting the further oxidation of -NH$_2$.

3.2. Crystal structure and textural properties

The effect of NaCl and KCl introduction on the crystal structure of CM catalyst was characterized by XRD (Fig. 2a). Pristine CM catalyst exhibited the characteristic diffraction peaks assigned to CrMn$_{1.5}$O$_4$ phase (PDF#71–0982). Relatively weak peaks ascribed to Cr$_2$O$_3$ phase (PDF#89–4836) and no extra diffractions ascribed to NaCl or KCl were observed (Chen et al., 2010). It indicated that NaCl and KCl were homogeneously dispersed on the CM catalyst surface or aggregated in tiny sizes that were beyond XRD detection limit (Liu et al., 2021b). However, the peak intensities of KCl$_{0.05}$-CM and NaCl$_{0.05}$-CM increased significantly, suggesting that there was strong interaction between NaCl/KCl and CM catalyst, and KCl and NaCl were beneficial for its crystallization (Li et al., 2019a).

N$_2$ adsorption-desorption experiments were conducted to further probe the effect of NaCl and KCl deposition on the textural properties of CM catalyst (Fig. 2b). All catalysts exhibited type IV isotherms with H3 type hysteresis loops, suggesting the appearance of mesoporous structure (Zheng et al., 2022). BET surface area, pore volume and pose size (Table 1) significantly reduced after NaCl and KCl introduction. It was because NaCl and KCl could block pore channel and cover the surface of CM catalyst, thereby suppressing the exposure of active sites (Li et al., 2020). Compare with NaCl$_{0.05}$-CM, KCl$_{0.05}$-CM with higher specific surface area exhibited lower NO conversion, indicating that specific surface area might not be the main reasons determining NH$_3$-SCR activity.

Fig. 1. NO conversion of CM, NaCl$_{0.05}$-CM and KCl$_{0.05}$-CM catalysts.

which peaks centered at 574.7–575.6, 575.4–576.7 and 577.4–578.4 eV were assigned to Cr^{2+}

3.3. Surface chemical properties

The influence of NaCl and KCl deposition on the valence states distribution of the surface atoms over CM catalyst was investigated by XPS. The XPS spectra of Cr $2p_{3/2}$ (Fig. 3a) could be separated into three peaks, among

Fig. 3. Cr 2p XPS spectra (a), Mn 2p XPS spectra (b), Optimized structures of oxygen vacancies (c), O 1 s XPS spectra (d), O_2-TPD profiles (e), H_2-TPD profiles (f) and optimized structures of alkali metal adsorption (Purple, gray, red, rose red, laurel-green and dark green balls represent Mn, Cr, O, Na, Cl and K, respectively.). (For interpretation of the references to colour in this figure legend, the reader is referred to the web version of this article.)

indicating that the activity of surface adsorbed oxygen ions/surface lattice oxygen for CM is superior to that of other catalysts (Shen et al., 2020). Compared with $NaCl_{0.05}$-CM catalyst, though intensities of the surface adsorbed oxygen ions/surface lattice oxygen peak were almost same, the bulk lattice oxygen peak of $KCl_{0.05}$-CM catalyst shifted to higher temperature range, thereby reducing bulk lattice oxygen activity. As a result, it could be safely concluded that both NaCl and KCl could decreased the activity of oxygen species and KCl could cause more severe poisoning on oxygen species than NaCl.

H_2-TPR experiments were carried out to assess the effect of NaCl and KCl on the redox properties of CM catalyst. As shown in Fig. 3f, all H_2-TPR curves consisted of two reduction peaks, which were attributed to the reduction of Mn_3O_4 to MnO (413/450 °C) and Cr_2O_3 to CrO (289/329/385 °C), respectively (Chen et al., 2010; Liu et al., 2020a). After adding NaCl and KCl, the peaks of Cr_2O_3 and Mn_3O_4 shifted higher temperature, indicating that NaCl and KCl could reduce the redox properties (Jiang et al., 2020b). Compared with $NaCl_{0.05}$-CM catalyst, the Cr_2O_3 peak of $KCl_{0.05}$-CM catalyst shifted lower temperature, but its total reduction peak area obviously reduced, which might be a reason further decreasing

redox properties. Reduced redox ability of CM catalyst by NaCl and KCl was responsible for well N_2 selectivity.

In this section, the effect of alkali metal adsorption on Mn\\O bond of CM catalyst was calculated, and the related models were shown in Fig. 3g. Na and K could adsorb stably on Q_c sites with adsorption energy of Š 2.184 and Š 2.594 eV, respectively. After Na and K adsorption, vicinal Mn\\O bond was enlarged from 2.030 to 2.097 and 2.109 Å, respectively, indicating that Na and K could weaken Mn\\O bond due to the electron transfer from Na and K to Mn, which might a vital cause declining the activity of Mn site (Jiang et al., 2021b; Shen et al., 2020). Cl could interact with metal sites including Cr and Mn, and Mn site exhibited lower adsorption energy (Š 2.482 eV) than Cr site (Š 1.678 eV), indicating that Mn site shown stronger affinity for Cl than Cr. Compared with Na and K adsorption, Mn\\O bond influenced by Cl was weaker due to less change of Mn\\O bond length. NaCl and KCl adsorbed on surface exhibited higher adsorption energy than single Na, K and Cl, indicating that the strong interaction between Na/K and Cl could diminish the interaction between Na/K with surface. However, the combination of Na/K and Cl did not alleviate the destruction of Mn\\O bond by single Na or K, and it still had a negative effect on Mn\\O bond.

3.4. Surface acidity properties

NH$_3$-TPD experiments were employed to explore the effect of NaCl and KCl on the surface acidity of CM catalyst. As shown in Fig. 4a, all catalysts possessed one common peak at 95 °C ascribed to NH$_4^+$ on Brønsted acid sites (Qin et al., 2022). However, CM catalyst exhibited another new strong peak at 352 °C attributed to coordinated NH$_3$ on Lewis acid sites (Liu et al., 2020b). After doping NaCl or KCl, Brønsted acid declined obviously and Lewis acid even disappeared, indicating that both NaCl and KCl could strongly interact with acid sites and suppress NH$_3$ adsorption (Jiang et al., 2020a). The NH$_3$-TPD peak areas were also calculated based on Fig. 4a and the results were shown in Table 1. The peak areas was ranked by CM > NaCl$_{0.05}$-CM > KCl$_{0.05}$-CM, indicating that both NaCl and KCl resulted in serious losses of acidity, and KCl exhibited stronger poison effect on surface acidity than NaCl.

In situ DRIFTS experiments were used to further investigate the effect of NaCl and KCl on surface acidity. For CM catalyst (Fig. 4b), several bands at 1200–1222, 1255, 1290, 1440, 1515, 1600, 1641, 3133–3376 cm^{-1} were detected. The bands at 1200–1222, 1255, 1290, 1600 cm^{-1} were attributed to NH$_3$ coordinated to Lewis acid sites (Xue et al., 2021; Yu et al., 2021). The bands at 1440/1641 cm^{-1} were ascribed to NH$_4^+$ ion bound to Brønsted acid sites (Zeng et al., 2020). The band at 1515 cm^{-1} was -NH$_2$ species due to the oxidation and decomposition of adsorbed NH$_3$ (Tan et al., 2020). Other bands at above 3100 cm^{-1} were related to the N—H bond stretching vibration of adsorbed NH$_3$ (Zhang et al., 2021). It could be observed that CM catalyst was dominated by abundant Lewis acid and Brønsted acid, and the amount of Brønsted acid was higher than Lewis acid at below 120 °C. However, with increasing temperature, Brønsted acid declined rapidly and hardly vanished at 120 °C, but Lewis acid almost changed, suggesting that Lewis acid was more stable than Brønsted acid (Huang et al., 2021). Furthermore, CM catalyst could exhibit excellent NH$_3$-SCR activity above 120 °C. Consequently, Lewis acid sites

Fig. 4. NH_3-TPD profiles (a), *in situ* DRIFTS spectra of NH_3 adsorption over CM (b), $NaCl_{0.05}$-CM (c) and $KCl_{0.05}$-CM (d) catalysts and optimized structures of NH_3 (e) and NH_4^+ (f) adsorption.

with Cr (-0.747 eV), indicating that Mn as main Lewis acid sites took part in NH_3-SCR reactions. After Na and K addition, the NH_3 adsorption energy on Mn site increased to -1.235 and -1.079 eV, respectively, demonstrating that both Na and K could slightly suppress NH_3 adsorption and decrease Lewis acid, and K had stronger inhibiting effect on Lewis acid formation than Na. However, compared with NH_3 adsorption, Cl showed stronger combining capacity with Mn (-2.482 eV), demonstrating that competitive adsorption between NH_3 and Cl on Mn site was a main reason reducing Lewis acid instead of Na and K. After NaCl and KCl introduction, KCl exhibited stronger inhibiting effect on Lewis acid formation than NaCl, but the poisoning effect of NaCl and KCl on Lewis acid was still weaker than single Na and K due to the strong interaction between Na/K and Cl.

NH_3 adsorbed on Brønsted acid sites (O site) in the form of NH_4^+, which was significant intermediate in NH_3-SCR reactions following L-H mechanism. As shown in Fig. 4f, NH_4^+ adsorb on O_{3c} exhibited lower adsorption energy (-3.365 eV) than Na and K on O_{3c}, indicating that O_{3c} exhibited stronger affinity to NH_4^+ instead of Na or K and Brønsted acid formation was not influenced by the competitive adsorption between Na/K and NH_4^+ on O_{3c}. After Cl addition, it was clear that NH_4^+ adsorption energy obviously decreased, indicating that Cl adsorption was unfavorable for Brønsted acid formation. NaCl and KCl exhibited almost same adsorption energy for NH_4^+ as Cl, illustrating that the interaction between Na/K and Cl hardly changed the negative effect of Cl on Brønsted acid.

3.5. Surface NO_x adsorption properties

In situ DRIFTS of $NO+O_2$ adsorption was used to explore the effect of NaCl and KCl on the formation of surface nitrates, and related results were shown in Fig. 5. For CM catalyst (Fig. 5a), several bands at 1205, 1434 and 1633 cm^{-1} were attributed to NO^- (Wei et al., 2018), linear nitrite (Liu et al., 2021d) and absorbed NO_2 (Pan et al., 2021b), respectively. The bands at 1295 and 1612 cm^{-1} belonged to monodentate nitrate (Nam et al., 2021; Wei et al., 2021). The bands at 1544 and 1569 cm^{-1} were ascribed to bidentate nitrate (Wang et al., 2021). Other bands at 1253, 1268 and 1353 cm^{-1} were related to bridged nitrate (Shi et al., 2021; Wu et al., 2021). Monodentate nitrate (1295 cm^{-1}) vanished with increasing temperature, but new band at 1253 and 1268 cm^{-1} arose, suggesting that monodentate nitrate was very unstable and could be easily converted into bridged nitrate. Similarly, the same phenomenon happened in the bands at 1434, 1544 and 1569 cm^{-1}, suggesting that unstable linear nitrate could be converted into bidentate nitrate. As reaction temperature increased to 160 °C, a new band (1633 cm^{-1}) emerged and remained stability above 160 °C, perhaps it was due to the continuous decomposition of monodentate nitrate.

In situ DRIFTS of $NO+O_2$ adsorption over $NaCl_{0.05}$-CM and $KCl_{0.05}$-CM were shown in Fig. 5b-c, respectively. The bands at 1263 and 1376 cm^{-1} were related to bridged nitrate. The bands at 1427 and 1612 cm^{-1}

$E_{ads}(NH_3)=-0.747$ eV $\qquad$ 325 eV $\qquad E_{ads}(NH_3)=-1.235$ eV
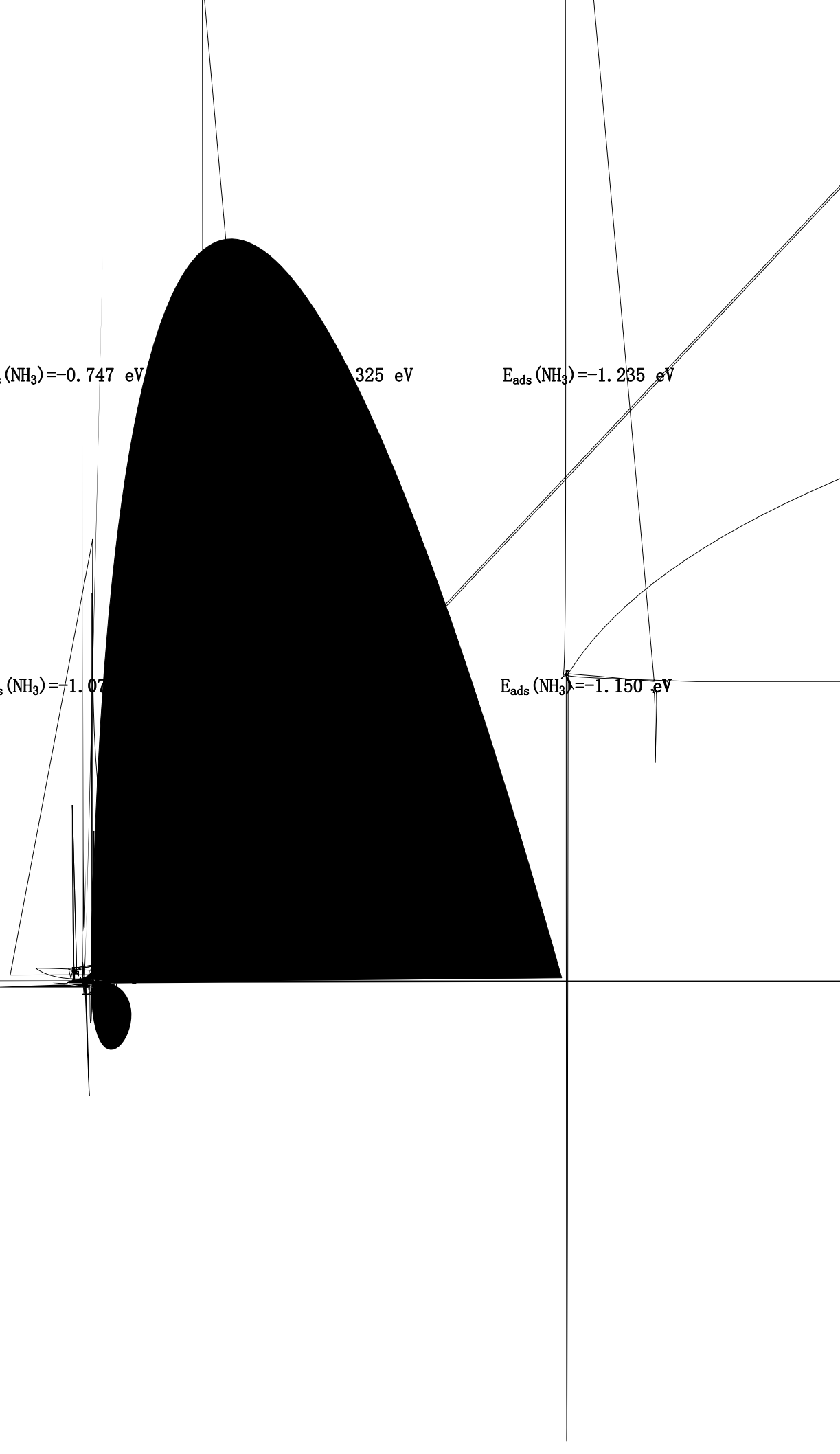
$E_{ads}(NH_3)=-1.07$ $\qquad E_{ads}(NH_3)=-1.150$ eV

belonged to linear nitrite and monodentate nitrate, respectively. The bands at 1627 and 1633 cm^{-1} were attributed adsorbed NO_2. With increasing temperature, all NO_x species except new band (1376 cm^{-1}) faded away. Compared with CM catalyst, NaCl and KCl obviously suppressed NO_x species adsorption and weakened their stability due to the interaction between NaCl/KCl and active sites, thereby inhibiting the formation of surface nitrates.

NO adsorption and activation influenced by NaCl and KCl were further investigated by DFT calculations. As shown in Fig. 5d, NO adsorption energy on Mn and Cr sites was -4.220 and -3.817 eV, respectively. Hence, Mn exhibited stronger affinity for NO than Cr. After Na and K addition, Na and K could weaken Mn—N bond, demonstrating that both Na and K could suppress NO adsorption/activation and hinder the formation of surface adsorbed NO_2 and nitrates. Compared with K effect, Na had weaker inhibiting effect on NO adsorption due to Na—O bond formation. With Cl further introduction, the poisoning effect of Na and K was ulteriorly receded, indicating that the interaction between Na/K and Cl could weaken the poisoning effect of Na and K on surface NO_x species.

3.6. Reaction mechanism

Transient reaction experiment was carried out to investigate the effect of NaCl and KCl on the reaction mechanism. For CM catalyst (Fig. 6a), after N_2 purge for 30 min, it was clear that abundant acid sites existed in CM catalyst, including Brønsted acid (1440 cm^{-1}), Lewis acid (1222 and 1600 cm^{-1}). In addition, -NH_2 species (1515 cm^{-1}

Fig. 6. *In situ* DRIFTS reactions between $NO+O_2$ and pre-adsorbed NH_3 over CM (a), $NaCl_{0.05}$-CM (b) and $KCl_{0.05}$-CM (c) catalysts at 160 °C, between NH_3 and pre-adsorbed $NO+O_2$ species over CM (d), $NaCl_{0.05}$-CM (e) and $KCl_{0.05}$-CM (f) catalysts at 160 °C and between NH_3 + $NO+O_2$ species over CM (g), $NaCl_{0.05}$-CM (h) and $KCl_{0.05}$-CM (i) catalysts.

Lewis acid by KCl and KCl. As a result, KCl could weaken NH_3 adsorption, but not change E-R mechanism of NH_3-SCR reactions.

Transient reaction experiment between pre-adsorbed $NO+O_2$ and NH_3 was carried out to further investigate the effect of NaCl and KCl on reaction mechanism, and the results were shown in Fig. 6. For CM catalyst (Fig. 6d), several bands at 1268/1353, 1544/1569 and 1633 cm^{-1} were attributed to bridged nitrate bands, bidentate nitrate bands and absorbed NO_2 band (1633 cm^{-1}) after $NO+O_2$ purging for 30 min. It was clear that the intensities of bands (1546, 1549 and 1633 cm^{-1}) increased with increasing time owing to the overlap of NH_4^+/-NH_2 and adsorbed NO_x species, respectively, indicating that adsorbed NO_x species was insert and could not interact with gaseous NO rapidly. As time increased to 10 min, bridged nitrate (1268 cm^{-1}) and absorbed NO_2 faded away, suggesting that some NH_3-SCR reactions between adsorbed NO_x and NH_3 species happened. Hence, CM catalyst followed Langmuir-Hinshelwood (L-H) mechanism (Wu et al., 2019).

As for $NaCl_{0.05}$-CM catalyst (Fig. 6e), there was only one band at 1400 cm^{-1} ascribed to liner nitrite after N_2 purge for 30 min. With increasing time, new band at 1608 cm^{-1} belonged to coordinated NH_3 on Lewis acid sites was observed, and the band at 1400 cm^{-1} originated from the overlap of NH_4^+ and liner nitrite, indicating that some reactions between adsorbed NO_x species and NH_3 species took place. Consequently, NaCl did not change L-H mechanism reactions of CM catalyst. But for $KCl_{0.05}$-CM catalyst (Fig. 6f), there was no band after N_2 purge for 30 min because KCl seriously suppressed the formation of adsorbed NO_x species.

$NH_3 + NO+O_2$ adsorption was carried out to further investigate the effect of NaCl and KCl on reaction mechanism during NH_3-SCR reactions. For CM catalyst (Fig. 6g), the bands at 1200/1222/1255/1600 and 1440/1469/1641 cm^{-1} were related to coordinated NH_3 on Lewis acid sites and NH_4^+ on Brønsted acid sites, respectively. Other bands at 1268/1353 and 1569 cm^{-1} were related to bridged nitrate and bidentate nitrate, respectively. In all temperature range, both active bidentate nitrate and bridged nitrate could interact with adsorbed NH_3 species, thereby demonstrating that NH_3-SCR reactions over CM catalyst adhered to L-H mechanism. Furthermore, active adsorbed NH_3 species could combine with gaseous NO. Consequently, NH_3-SCR reactions over CM catalyst also followed E-R mechanism.

For $NaCl_{0.05}$-CM catalyst (Fig. 6h), the bands at 1427, 1544, 1602 and 1645 cm^{-1} were ascribed to linear nitrite, -NH_2 species, coordinated NH_3 and NH_4^+, respectively. Adsorbed NO_x species interacted with adsorbed NH_3 species. It was demonstrated that NH_3-SCR reactions over $NaCl_{0.05}$-CM catalyst complied with L-H mechanism. As for $KCl_{0.05}$-CM catalyst (Fig. 6i), the bands at 1162, 1430, 1247 and 1616 cm^{-1} were attributed to coordinated NH_3, NH_4^+, bridged nitrate and monodentate nitrate, respectively. With increasing temperature, new band at 1386 cm^{-1} attributed to bridged nitrate could be observed. NH_3-SCR reactions between adsorbed NH_3 and NO_x species existed, and NH_3-SCR reactions over $KCl_{0.05}$-CM catalyst complied with L-H mechanism. Moreover, active adsorbed NH_3 species combined with gaseous NO, thereby also demonstrating that NH_3-SCR reactions over $KCl_{0.05}$-CM catalyst also complied with E-R mechanism.

3.7. Reaction steps

3.7.1. E-R mechanism

According to the calculated results of NH_3 adsorption, NH_3 could stably adsorb on Mn site. Accordingly, NH_3-SCR reaction pathways (E-R mechanism) over CM catalyst were calculated, and the related models and reaction energy profile were shown in Fig. 7a-b. NH_3 adsorption/ decomposition was the first step in simulating E-R mechanism reactions. NH_3 molecule anchored in Mn site by its N atom to form a stable intermediate structure (denoted as IM1). Soon afterwards, one H atom of NH_3 molecule moved to nearby location, and NH_2 group was close to Mn atom to form the second intermediate structure, namely IM2. In IM2, N\—\Mn bond shrank from 2.175 to 1.935 Å. The reaction step (IM1 to IM2) was endothermic by 0.123 eV and need to overcome 2.383 eV energy barrier to reach transition state (TS1). Gaseous NO molecule was gradually close to

Fig. 6 (continued).

NH$_2$ group to from ONNH$_2$ intermediate, namely IM3. In IM3, O atom of NO was connected to Mn atom and Cr atom, and N‒Mn bond was further enlarged from 1.935 to 2.163 Å. This process (IM2→TS2→IM3) was endothermic by 2.964 eV, corresponding to Š 0.919 eV energy barrier (TS2), indicating that this process was spontaneous. ONNH$_2$ intermediate was continually dehydrogenated one H atom and converted into HONNH intermediate (IM4). In this process (IM3 to IM4), one H atom of NH$_2$ transferred and combined with O atom of ON. The transfer step of related H atom was endothermic by 3.045 eV, corresponding to energy barrier (TS3) of 0.648 eV. Based on IM4, the N‒O and N‒H bonds of HONNH intermediate ruptured, and one H atom was transferred to connect to O atom and another N atom to form stable H$_2$ONN intermediate (IM5). This isomerization process was endothermic by 9.97 eV and need to overcome 7.074 eV en423.5((3)0(15.1(131 5((3)0(13(3)-2i)-15--200.1(t)0(h19.6(y.7(e)-8.1)0(15.1(133)-2i410.

(d)

IM1   TS1   IM2

TS2   IM3   TS3

IM4   TS4   IM5
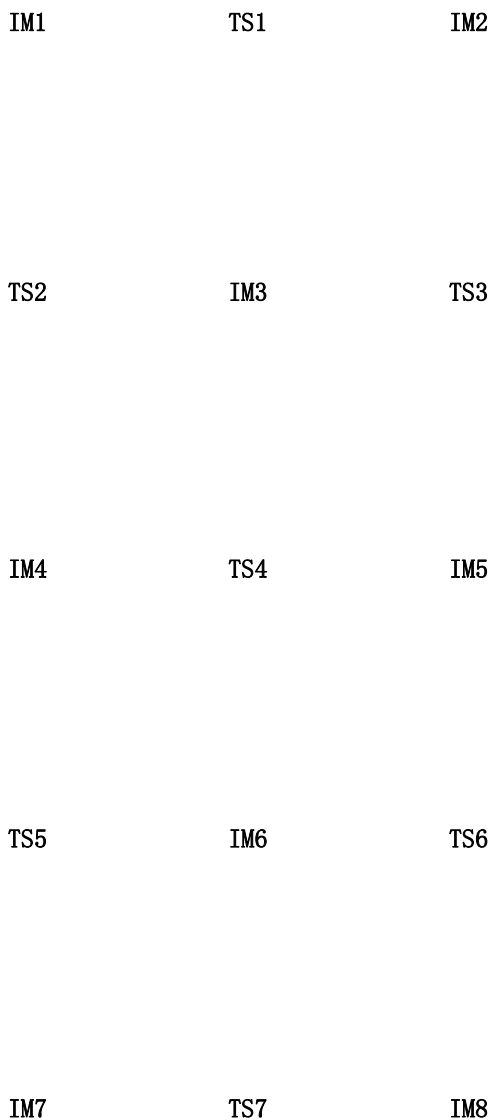
TS5   IM6   TS6

IM7   TS7   IM8

Fig. 7 (continued).

corresponding to energy barrier of 0.967 and 1.102 eV that had to overcome, respectively. Compared with CM catalyst, NaCl and KCl reduced its reaction energy barrier of rate-controlling step, but increased its reaction heat. It indicated that reaction heat of rate-controlling step might be a vital reason poisoning CM catalysts in NH_3-SCR reactions that followed E-R mechanism.

3.7.2. L-H mechanism

In situ DFIFTS results demonstrated that CM catalyst could promote the oxidization of NO into NO_2, and formed NO_2 interacted with NH_4^+ on Brønsted acid sites to produce NH_4NO_2 and then was further decomposed into N_2 and H_2O, which adhered to L-H mechanism. In this section, the reactions between NH_4^+ and NO_2 was further investigated by DFT calculations, and related geometric structures and energy changes were shown in Fig. 7d-e. NH_4^+ and NO_2 were adsorbed on Q_{8c} and Mn site stably,

respectively, to form NH_4NO_2 structure (IM1). Subsequently, one H atom of NH_4^+ gradually approached O atom of NO_2 to form the NH_3NO_2H intermediate (IM2). At the same time, H-O_{3c} bond and N↖Mn bond were enlarged from 1.021 to 1.856 Å and 2.041 to 2.054 Å, respectively. In the process of H atom transfer, the reaction was endothermic by 0.245 eV and need to overcome 0.360 eV energy barrier. Then one O atom of HNO_2 continued to take away one H atom of NH_3 to form the $NH_2NO_2H_2$ intermediate (IM3). In this process (IM2↖TS2↖IM3), N↖H bond of NH_3 (IM2) was broke, and related H atom was gradually closed to one O atom. Simultaneously, N↖O bond of HNO_2 was broke, and another H atom combined with one O atom to form O-H-O bond and one H_2O molecule. This process (H_2O formation) was endothermic by 1.705 eV, corresponding to 3.793 eV energy barrier. Subsequently, one H_2O molecule was desorbed form the matrix to form IM4 intermediate, and this process was endothermic by 5.992 eV, corresponding to 5.414 eV barrier energy.

One H atom of formed NH_2NO structure in IM4 continually escaped and gradually approached to one O atom of NH_2NO to form NHNOH structure (IM5), which was endothermic by 0.122 eV and overcome 2.153 eV barrier energy. Based on IM5, Q_{3c}-H-N bond was gradually enlarged and broken, and N atom of NNOH got one H atom from O_1 H bond, then O_1 N bond was broken and O attracted two H atom to form one H_2O molecule. In the process of H_2O formation (IM5 TS5 IM6), the reaction was exothermic by 1.726 eV and the reaction energy was 1.928 eV. Soon afterwards, H_2O and N_2 was desorbed one by one to form IM7 and IM8, which was endothermic by 2.837 and 3.175 eV, corresponding to energy barrier of 6.085 and 0.875 eV, respectively. It was obvious that the reaction energy barrier of H_2O desorption process (IM6 TS6 IM7) was the highest, indicating that H_2O desorption was also the rate-controlling step of NH_3-SCR reaction that followed L-H mechanism. The effect of alkali on this rate-controlling step was further investigated, and the results were shown in Fig. 7f. In IM6, Na (K) and Cl could stably adsorb on O_{3c} and Mn site, respectively, and O atom of H_2O was closed to one N atom of N_2 on Mn site to form a stable intermediate (IM6). Soon afterwards, the distance between N and O atoms gradually enlarged and H_2O gradually escaped from the matrix to form the next intermediate (IM7). This rate-controlling process was endothermic by Š 0.089 ($NaCl_{0.05}$-CM) and 0.931 eV ($KCl_{0.05}$-CM), corresponding to energy barrier of 1.091 and 7.547 eV that had to overcome, respectively. Compared with CM catalyst, NaCl not only decreased reaction heat of rate-controlling step, but also reduce its reaction energy barrier, indicating that reaction energy barrier and reaction heat were not reasons poisoning CM catalyst by NaCl. Compared with CM catalyst, though KCl reduced its reaction heat of rate-controlling step, but increased its reaction energy barrier. It indicated that reaction energy barrier of rate-controlling step might be a vital reason poisoning CM catalysts by KCl in NH_3-SCR reactions that followed L-H mechanism.

4. Conclusions

In summary, we successfully illustrated the poisoning mechanism of CM catalyst by alkali metals by experiments and DFT calculations. The characterizations unveiled that NaCl and KCl could make a decrease in specic surface area, electron transfer (Cr^{5+} +Mn^{3+} Cr^{3+} +Mn^{4+}), redox ability, oxygen vacancies formation, NH_3 adsorption, the stability of Brønsted/Lewis acid and surface NO_x species variety, amount and stability.

Li, Y., Yang, S., Peng, H., Liu, W., Mi, Y., Wang, Z., Tang, C., Wu, D., An, T., 2021b. Insight into the activity and SO2 tolerance of hierarchically ordered MnFe1-δCoδOx ternary oxides for low-temperature selective catalytic reduction of NOx with NH3. J. Catal. 395, 195–209.

Lian, Z., Liu, L., Lin, C., Shan, W., He, H., 2022. Hydrothermal aging treatment activates V2O5/TiO2 catalysts for NOx abatement. Environ. Sci. Technol. 56, 9744–9750.

Liu, Y.-Z., Guo, R.-T., Duan, C.-P., Wu, G.-L., Miao, Y.-F., Gu, J.-W., Pan, W.-G., 2020a. highly effective urchin-like MnCrOx catalyst for the selective catalytic reduction of NOx with NH3. Fuel 271, 117667.

Liu, Z., Chen, C., Zhao, J., Yang, L., Sun, K., Zeng, L., Pan, Y., Liu, Y., Liu, C., 2020b. Study on the NO2 production pathways and the role of NO2 in fast selective catalytic reduction DeNOx at low-temperature over MnOx/TiO2 catalyst. Fuel 271, 117667.

Liu, B., Liu, J., Xin, L., Zhang, T., Xu, Y., Jiang, F., Liu, X., 2021a. Unraveling reactivity descriptors and structure sensitivity in low-temperature NH3-SCR reaction over CeTiOx catalysts: a combined computational and experimental study. ACS Catal. 11, 7613–7636.

Liu, J., Cheng, H., Zheng, H., Zhang, L., Liu, B., Song, W., Liu, J., Zhu, W., Li, H., Zhao, Z., 2021b. Insight into the potassium poisoning effect for selective catalytic reduction of NOx with NH3 over Fe/beta. ACS Catal. 11, 14727–14739.

Liu, J., Ren, X., Zhang, Z., Sun, N., Tan, H., Cai, J., 2021c. Study on the mechanism of selective catalytic reduction of NOx by NH3 over Mn-doped CoCr2O4. J. Phys. Chem. C 125, 14228–14238.

Liu, J., Wu, X., Hou, B., Du, Y., Liu, L., Yang, B., 2021d. NiMn2O4 sphere catalyst for the selective catalytic reduction of NO by NH3: insight into the enhanced activity via solvothermal method. J. Environ. Chem. Eng. 9, 105152.

Lyu, Z., Niu, S., Lu, C., Zhao, G., Gong, Z., Zhu, Y., 2020. A density functional theory study on the selective catalytic reduction of NO by NH3 reactivity of α-Fe2O3 (001) catalyst doped by mn, tiCr and Ni. Fuel 267, 117147.

Nam, K.B., Lee, S.H., Hong, S.C., 2021. The role of copper in the enhanced performance of W/Ti catalysts for low-temperature selective catalytic reduction. Appl. Sur. Sci. 544, 148643.

Pan, H., Gao, E.-H., Fang, T.-T., Mei, Y., He, Y., Shi, Y., 2021a. in situ treatment by high-temperature water vapor as a novel health-care approach for commercial SCR catalyst. Appl. Sur. Sci. 541, 148408.

Pan, Y., Jin, Q., Lu, B., Ding, Y., Xu, X., Shen, Y., Zeng, Y., 2021b. New insights into MnCe(Ba) O/TiO2 composite oxide catalyst: barium additive accelerated ammonia conversion. J. Rare. Earth. 39, 532–540.

Peng, Y., Li, J., Chen, L., Chen, J., Han, J., Zhang, H., Han, W., 2012a. Alkali metal poisoning of a CeO2-WO3 catalyst used in the selective catalytic reduction of NOx with NH3: an experimental and theoretical study. Environ. Sci. Technol. 46, 2864–2869.

Peng, Y., Li, J., Shi, W., Xu, J., Hao, J., 2012b. Design strategies for development of SCR catalyst: improvement of alkali poisoning resistance and novel regeneration method. Environ. Sci. Technol. 46, 12623–12629.

Qin, G., Zheng, J., Li, Y., Yang, Y., Liu, X., Han, X., Huang, Z., 2022. Tailor the crystal planes of MIL-101(Fe) derivatives to enhance the activity of SCR reaction at medium and low temperature. J. Colloid Interface Sci. 615, 432–444.

Ren, D., Gui, K., Gu, S., 2021. Quantum chemistry study of SCR-NH3 nitric oxide reduction on ce-doped γFe2O3 catalyst surface. Mol. Catal. 502, 111373.

Shen, Y., Deng, J., Impeng, S., Li, S., Yan, T., Zhang, J., Shi, L., Zhang, D., 2020. Boosting toluene combustion by engineering co-O strength in cobalt oxide catalysts. Environ. Sci. Technol. 54, 10342–10350.

Shi, Y., Yi, H., Gao, F., Zhao, S., Xie, Z., Tang, X., 2021e. Evolution mechanism of transition metal in NH3-SCR reaction over Mn-based bimetallic oxide catalysts: structure-activity relationships. J. Hazard. Mater. 413, 125361.

Tan, W., Wang, J., Li, L., Liu, A., Song, G., Guo, K., Luo, Y., Liu, F., Gao, F., Dong, L., 2020. Gas phase sulfation of ceria-zirconia solid solutions for generating highly efficient and SO2 resistant NH3-SCR catalysts for NO removal. J. Hazard. Mater. 388, 121729.

Wang, S.-X., Guo, R.-T., Pan, W.-G., Chen, Q.-L., Sun, P., Li, M.-Y., Liu, S.-M., 2017. The deactivation of Ce/TiO2 catalyst for NH3-SCR reaction by alkali metals: TPD and DRIFT studies. Catal. Commun. 89, 143–147.

Wang, Z., Lan, J., Haneda, M., Liu, Z., 2021. Selective catalytic reduction of NOx with NH3 over a novel Co-Ce-Ti catalyst. Catal. Today 376, 222–228.

Wei, Y., Fan, H., Wang, R., 2018. Transition metals (Co, zr, Ti) modified iron-samarium oxide as efficient catalysts for selective catalytic reduction of NOx at low-temperature. Appl. Sur. Sci. 459, 63–73.

Wei, L., Wang, Z., Liu, Y., Guo, G., Dai, H., Cui, S., Deng, J., 2021. Support promotion effect on the SO2 and K(+) co-poisoning resistance of MnO2/TiO2 for NH3-SCR of NO. J. Hazard. Mater. 416, 126117.

Wu, Z., Zeng, Y., Song, F., Zhang, S., Zhong, Q., 2019. Active sites assembly effect on CeO2-WO3-TiO2 catalysts for selective catalytic reduction of NO with NH3. Mol. Catal. 479, 110549.

Wu, G.-L., Guo, R.-T., Liu, Y.-Z., Duan, C.-P., Miao, Y.-F., Gu, J.-W., Pan, W.-G., 2021. Promoting effect of Sb on the selective catalytic reduction of NO with NH3 over CeVO4 catalyst. J. Energy Inst. 95, 77–86.

Xie, A., Tang, Y., Huang, X., Jin, X., Gu, P., Luo, S., Yao, C., Li, X., 2019. Three-dimensional nano ower MnCrO/sepiolite catalyst with increased SO2 resistance for NH3-SCR at low temperature. Chem. Eng. J. 370, 897–905.

Xue, H., Guo, X., Meng, T., Guo, Q., Mao, D., Wang, S., 2021. Cu-ZSM-5 catalyst impregnated with Mn–Co oxide for the selected catalytic reduction of NO: physicochemical property-catalytic activity relationship and in situ DRIFTS study for the reaction mechanism. ACS Catal. 11, 7702–7718.

Yao, X., Chen, L., Cao, J., Chen, Y., Tian, M., Yang, F., Sun, J., Tang, C., Dong, L., 2019. Enhancing the deNO performance of MnO/CeO2-ZrO2 nanorod catalyst for low-temperature NH3-SCR by TiO2 modi cation. Chem. Eng. J. 369, 46–56.

Yoon, W., Kim, Y., Jong Kim, G., Kim, J.-R., Lee, S., Han, H., Hyeon Park, G., Chae, H.-J., Bae Kim, W., 2022. Boosting low temperature De-NOx performance and SO2 resistance over Ce-doped two dimensional Mn-Cr layered double oxide catalyst. Chem. Eng. J. 434, 134676.

Youn, J.-R., Kim, M.-J., Lee, S.-J., Ryu, I.-S., Yoon, H.C., Jeong, S.K., Lee, K., Jeon, S.G., 2021. The in uence of CNTs addition on Mn-Ce/TiO2 catalyst for low-temperature NH3-SCR of NO. Catal. Commun. 152, 106282.

Yu, Y., Tan, W., An, D., Tang, C., Zou, W., Ge, C., Tong, Q., Gao, F., Sun, J., Dong, L., 2021. Activity enhancement of WO3 modi ed FeTiO catalysts for the selective catalytic reduction of NO by NH3. Catal. Today 375, 614–622.

Zeng, Y., Song, W., Wang, Y., Zhang, S., Wang, T., Zhong, Q., 2020. Novel fe-doped CePO4 catalyst for selective catalytic reduction of NO with NH3: the role of Fe(3+) ions. J. Hazard. Mater. 383, 121212.

Zhang, J., Liang, J., Peng, H., Mi, Y., Luo, P., Xu, H., He, M., Wu, P., 2021. Cost-effective fast-synthesis of chabazite zeolites for the reduction of NOx. Appl. Catal. B-Environ. 292, 120163.

Zheng, W., Zhang, X., Zheng, Y., Yue, Y., 2022. "Oxynitride trap" over N/S co-doped graphene-supported catalysts promoting low temperature NH3-SCR performance: insight into the structure and mechanisms. J. Hazard. Mater. 423, 127187.